

# On microscopic theory of radiative nuclear reaction characteristics

S. Kamerdzhev

*National Research Centre "Kurchatov Institute", Moscow, Russia*

O. Achakovskiy\* and A. Avdeenkov

*Institute for Physics and Power Engineering, 249033 Obninsk, Russia*

S. Goriely

*Institut d'Astronomie et d'Astrophysique, ULB, CP 226, B-1050 Brussels, Belgium*

A survey of some results in the modern microscopic theory of properties of nuclear reactions with gamma-rays is given. First of all, we discuss the impact of phonon coupling (PC) on the photon strength function (PSF) because it represents the most natural physical source of additional strength found for Sn isotopes in recent experiments that could not be explained within the standard HFB+QRPA approach. The self-consistent version of the Extended Theory of Finite Fermi Systems in the Quasiparticle Time Blocking Approximation, or simply QTBA, is applied. It uses the HFB mean field and includes both the QRPA and PC effects on the basis of the SLy4 Skyrme force. With our microscopic E1 PSFs, the following properties have been calculated for many stable and unstable even-even semi-magic Sn and Ni isotopes as well as for double-magic  $^{132}\text{Sn}$  and  $^{208}\text{Pb}$  using the reaction codes EMPIRE and TALYS with several nuclear level density (NLD) models: 1) the neutron capture cross sections, 2) the corresponding neutron capture gamma spectra, 3) the average radiative widths of neutron resonances. In all the properties considered, the PC contribution turned out to be significant, as compared with the standard QRPA one, and necessary to explain the available experimental data. The results with the phenomenological so-called generalized superfluid NLD model turned out to be worse, on the whole, than those obtained with the microscopic HFB+combinatorial NLD model. The very topical question about the M1 resonance contribution to PSFs is also discussed.

Finally, we also discuss the modern microscopic NLD models based on the self-consistent HFB method and show their relevance to explain experimental data as compared with the phenomenological models. The use of these self-consistent microscopic approaches is of particular relevance for nuclear astrophysics, but also for the study of double-magic nuclei.

PACS numbers: 24.10.-i, 24.60.Dr, 24.30.Cz, 21.60.Jz

## I. INTRODUCTION

In order to calculate characteristics of nuclear reactions with gamma-rays, information on the photon strength function (PSF) and nuclear level density (NLD) models is necessary. Traditionally, these quantities have been modeled phenomenologically and the corresponding parameters adjusted on stable nuclei. Such information is needed to calculate all characteristics of nuclear reactions with gamma-rays, in particular, the radiative neutron capture cross sections of particular interest in astrophysical [1] and nuclear engineering [2] applications. Commonly, one parametrizes the PSF phenomenologically using, for example, Lorentzian-type models [3, 4]. The usual definition of PSF contains transitions between excited states. For this reason, in order to calculate the PSF, the known Brink hypothesis [5] is often used which states that on each excited state it is possible to build a giant dipole resonance (at present, any giant resonance) including its low-lying part. In the low-lying energy region, there exists the so-called Pygmy Dipole Resonance (PDR). It ex-

hausts typically about 1-2% of the Energy Weighted Sum Rule (EWSR) but, nevertheless, it can significantly increase the radiative neutron capture cross section and affect the nucleosynthesis of neutron-rich nuclei by the r-process [1]. In neutron-rich nuclei, for example,  $^{68}\text{Ni}$  [6] and, probably,  $^{72,74}\text{Ni}$ , the PDR fraction of the EWSR is expected to be much larger. Note that for nuclei with small neutron separation energy, less than typically 3–4 MeV, the PDR properties are changed significantly [1], and therefore, phenomenological systematics obtained by fitting characteristics of stable nuclei cannot be applied. Through the Brink hypothesis [5], the de-excitation PSF is directly connected to the photoabsorption cross section and, therefore, with the PDR field [3, 7, 8]. For all these reasons, during the last decade there has been an increasing interest in the investigations of the excitations in the PDR energy region manifested both in "pure" low-energy nuclear physics [7, 9] and in the nuclear data field [1, 3, 4].

The experiments in the PDR energy region [10–13] have given additional information about the PDR and PSF structures. The PSF structures at 8–9 MeV in six Sn isotopes obtained by the Oslo method [10, 11] could not be explained within the standard phenomenological approach. In order to explain the experiment, it was

---

\*oachakovskiy@ippe.ru

necessary to add "by hand" some additional low-lying strength of about 1–2% of the EWSR.

Given the importance of PSF both in astrophysics [1] and nuclear engineering [2], microscopic investigations are required, especially when extrapolations to exotic nuclei are needed. Mean-field approaches using effective nucleon interactions, such as the Hartree-Fock Bogoliubov method and the quasi-particle random-phase approximation (HFB+QRPA) [1], allow systematic self-consistent studies of isotopic chains, and for this reason have been included in modern nuclear reaction codes like EMPIRE [14] or TALYS [15]. Such an approach is of higher predictive power in comparison with phenomenological models. However, as we discuss below, and as confirmed by recent experiments, the HFB+QRPA approach is necessary but not sufficient. To be exact, it should be complemented by the effect describing the interaction of single-particle degrees of freedom with the low-lying collective phonon degrees of freedom, known as the phonon coupling (PC).

The results in Ref. [13] directly confirm the necessity to go beyond the HFB+QRPA method because the PSF structures observed in Ref. [11] could not be explained within the HFB+QRPA approach. In particular, the PC effects discussed in Refs.[8, 16, 17] may be at the origin of such an extra strength. Note that the microscopic PSFs which contained transitions between the ground and excited states, i.e. the PSFs values at the energy point near the neutron separation energy, have already been estimated long ago within the quasiparticle-phonon model approach, which also includes the PC [18].

There are also some additional questions for double-magic nuclei. The problem is that the phenomenological approaches "smooth" the individual characteristics of these nuclei or consider them on average. Individual peculiarities are especially expressive just for double-magic nuclei, even for stable, not to mention unstable ones. For example, to include the vibrational NLD enhancement to the well-known generalized superfluid model (GSM) [3, 4], the experimental values for the energies of the first  $2^+$  and the approximate  $50A^{-2/3}$  MeV energies for the first  $3^-$  levels are usually considered. Such a formula is however not suited for double-magic nuclei, and both these prescriptions should not be used for unstable nuclei. Microscopic approaches in nuclear theory account for the specificity of each nucleus through its single-particle and collective (phonon) properties. Therefore, it allows for some irregular changes in comparison with global phenomenological models [19] to be seen and checked. Thus, for double-magic nuclei it is especially necessary to use microscopic approaches for both the PSF and NLD.

Many different NLD models have been developed for the last decades and in many respect NLD predictions are still not satisfactory, especially in view of their importance in reaction modelling. The shortcomings of analytical NLD formulae in matching experimental data are overcome, as a rule, by empirical parameter adjustments. For this reason, their predictive power away from experimental constraints is questionable in contrast to more mi-

croscopic approaches that have been seriously developed for the last decades. The present paper also reviews the last attempt made to improve microscopic NLD models for practical applications.

In this work we discuss and compare i) the microscopic and phenomenological PSF models, ii) the corresponding radiative nuclear reaction characteristics, namely, the neutron radiative capture cross sections, the corresponding capture  $\gamma$ -ray spectra and average radiative widths, iii) phenomenological and microscopic NLD models required for calculations of these radiative nuclear reaction characteristics. To estimate PSFs, we use the self-consistent version of the extended theory of finite fermi systems (ETFFS) [16] in the quasi-particle time blocking approximation (QTBA) [20]. Our ETFFS (QTBA) method, or simply QTBA, includes self-consistently the QRPA and PC effects and the single-particle continuum in a discrete form. Details of the method are described in Ref. [17]. The method allows us to investigate the impact of the PC on nuclear reaction in both stable and unstable nuclei. We calculate the microscopic PSFs in several Sn and Ni isotopes as well as (due to their above-mentioned specificities) in the doubly-magic nuclei  $^{132}\text{Sn}$  and  $^{208}\text{Pb}$  and use them in the EMPIRE and TALYS codes to estimate the neutron capture cross sections, the corresponding capture gamma-ray spectra and the average radiative widths. Finally, in view of the importance of NLD in reaction theory, a review on the last developments made to determine NLD within the mean field plus combinatorial model is given in Sect. VII.

## II. METHOD

The strength function  $S(\omega) = dB(E1)/d\omega$  [16, 17], related to the PSF  $f(E1)$  by  $f(E1, \omega)[\text{MeV}^{-3}] = 3.487 \cdot 10^{-7} S(\omega)[\text{fm}^2 \text{MeV}^{-1}]$ , is calculated by the QTBA method [16, 20] on the basis of the SLy4 Skyrme force [21]. The ground state is calculated within the HFB method using the spherical code HFBRAD [22]. The residual interaction for the (Q)RPA and QTBA calculations is derived as the second derivative of the Skyrme functional. In all our calculations we use a smoothing parameter of 200 keV which effectively accounts for correlations beyond the considered PC. Such a choice guarantees a proper description of all three characteristics of giant resonances, including the width [16], and also corresponds to the experimental resolution of the Oslo method [11].

## III. PSF'S AND PDR'S

### A. Sn and Ni isotopes

In Figs. 1 and 2, the E1 PSFs for three even-even Sn isotopes are compared with experimental data obtained with the Oslo method [11] for Sn isotopes as well as with

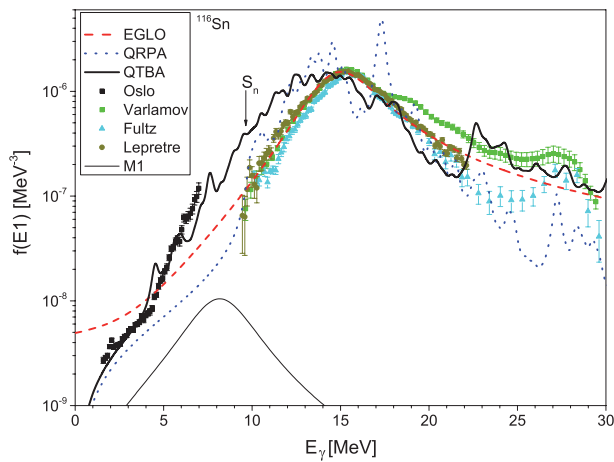


FIG. 1: The E1 photon strength functions for  $^{116}\text{Sn}$ . The dashed lines are obtained with the EGLO model [3], the dotted line corresponds to the QRPA calculation, and the solid line to QTBA calculation. The arrow marks the neutron separation energy  $S_n$ . The experimental data are taken from [10, 23–25].

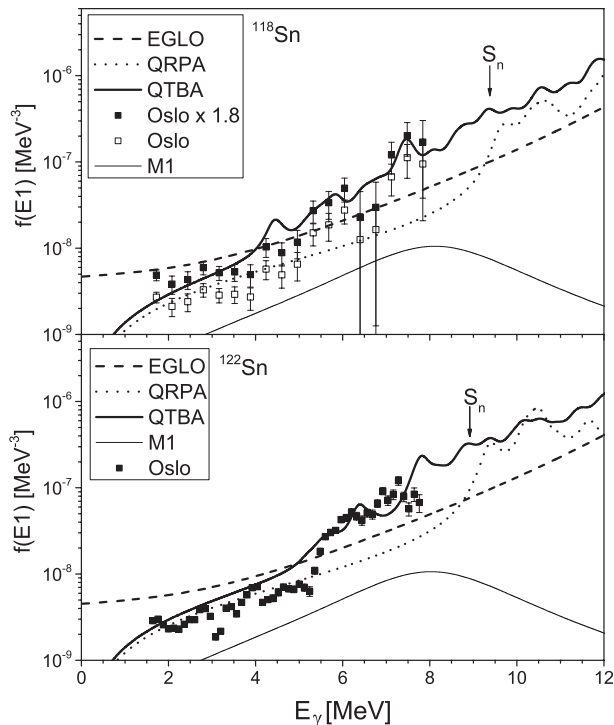


FIG. 2: Same as Fig. 1, but for  $^{118}\text{Sn}$  and  $^{122}\text{Sn}$  within the PDR energy region. The experimental data are taken from [10, 11].

the phenomenological Enhanced Generalized Lorentzian (EGLO) model [3]. It can be seen that *i*) in contrast to phenomenological models, the structure patterns caused by both the QRPA and PC effects are pronounced in both Sn and Ni isotopes. Physically, the PC structures are caused by the poles at  $\omega = \epsilon_1 - \epsilon_2 - \omega_s$  or  $\omega = E_1 + E_2 - \omega_s$ ,

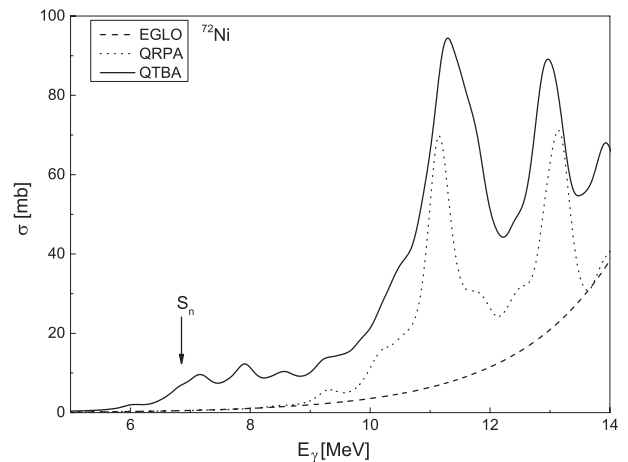


FIG. 3: The calculated photoabsorption cross section in  $^{72}\text{Ni}$

where  $\epsilon_1, E_1, \omega_s$  are single-particle, quasi-particle and phonon energies, respectively. Such a PC effect is seen to become significant above 3 MeV and below typically 9–10 MeV; *ii*) for  $^{118}\text{Sn}$  and  $^{122}\text{Sn}$  isotopes, a reasonable agreement with experiment is obtained within the QRPA below typically 5 MeV. For all three Sn isotopes, at  $E > 5$  MeV, the inclusion of PC effects is needed to reconcile predictions with experiment [11]; *iii*) up to the nucleon separation energy, the phenomenological EGLO description of the experimental data is noticeably worse than the one achieved by the QTBA.

In Table I, the integral parameters (mean energy  $E$  and fraction of EWSR exhausted) of the PDR are given for three Ni isotopes, as predicted by both QRPA and QTBA models. To compare results in these three nuclei, a 6 MeV energy interval, which corresponds to the one where the PDR was observed in  $^{68}\text{Ni}$ , is considered. In this interval, the PDR characteristics have been approximated, as usually, with a Lorentz curve by fitting the three moments of the theoretical curves [16]. For  $^{68}\text{Ni}$ , a good agreement is obtained with experimental data of the mean energy  $E \simeq 11$  MeV and about 5% of the total EWSR [6]. A similar calculation was performed for  $^{68}\text{Ni}$  [26] using the relativistic QTBA, with two phonon contributions additionally taking into account. For the PDR characteristics in  $^{72}\text{Ni}$  in the (8-14) MeV range, we obtain a mean energy  $E = 12.4$  MeV, width  $\Gamma = 3.5$  MeV and a large strength of 25.7% of the EWSR. It should be noted that the main contribution to the  $^{72}\text{Ni}$  PDR is found in the (10-14) MeV interval which exhausts 13.9% of the EWSR for QRPA and 23.2% for QTBA. In this interval, two maxima can be observed (Fig 3). So the strength in the (10-14) MeV dominates and is globally equivalent to the one in (8-14) MeV. A significant PC contribution to the PDR strength is found in all isotopes (Table I).

TABLE I: Integral characteristics of the PDR (mean energy  $E$  in MeV and fraction of the EWSR) in Ni isotopes calculated in the (8-14) MeV interval for  $^{58}\text{Ni}$ ,  $^{72}\text{Ni}$  and (7-13) MeV interval for  $^{68}\text{Ni}$  (see text for details).

Nuclei	QRPA		QTBA	
	$E$	%	$E$	%
$^{58}\text{Ni}$	13.3	6.0	14.0	11.7
$^{68}\text{Ni}$	11.0	4.9	10.8	8.7
$^{72}\text{Ni}$	12.4	14.7	12.4	25.7

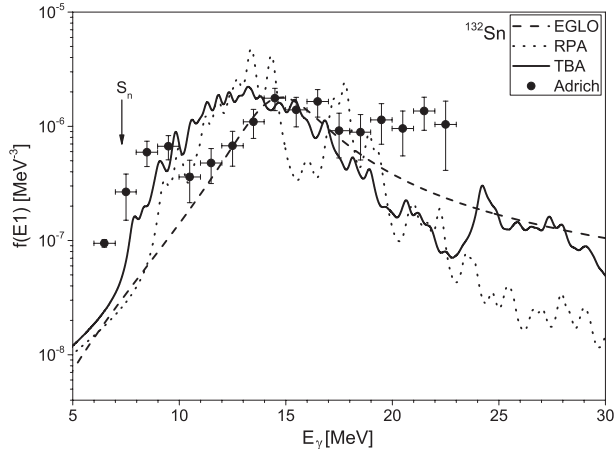


FIG. 4: The PSF for  $^{132}\text{Sn}$ . Dotted lines correspond to the self-consistent RPA, solid lines to the TBA (including PC), and dashed lines to the EGLO model [3]. Experimental data [28] were recalculated by us for PSF.

## B. Double-magic $^{132}\text{Sn}$ and $^{208}\text{Pb}$

In Figs. 4 and 5, we show the PSFs for  $^{132}\text{Sn}$  and  $^{208}\text{Pb}$  calculated within our microscopic TBA and RPA methods with the SLy4 Skyrme force. These PSFs are recalculated from the theoretical photoabsorption cross sections taken from Ref. [17] ( $^{132}\text{Sn}$ ) and [27] ( $^{208}\text{Pb}$ ). Note that for the first time, the microscopic PSFs are obtained within the fully self-consistent approach with an exact account for the single-particle continuum (for  $^{208}\text{Pb}$ ). The phenomenological EGLO PSFs are also shown. In Fig. 4, the E1 PSF for  $^{132}\text{Sn}$  is compared with experimental data from Ref. [28]. In Fig. 5, the E1 PSF for  $^{208}\text{Pb}$  is compared with the experimental data obtained within the Oslo method [29]. As can be seen, in contrast to the phenomenological model EGLO and microscopic continuum RPA, the CTBA, i.e. RPA + PC, can describe some PDR structures in  $^{132}\text{Sn}$  and partly in  $^{208}\text{Pb}$  thanks to the PC effects. For  $^{132}\text{Sn}$ , we see the well-known structure at about 10 MeV (our approach gives a lower energy), usually referred to as a PDR for the photoabsorption cross section, as discussed in Refs. [7, 9, 17].

Let us discuss the results shown in Fig. 5 for  $^{208}\text{Pb}$ . We see that the CTBA approach describes relatively well experimental data at  $E > 5$  MeV, at least better than the CRPA model (note that the smoothing parameter

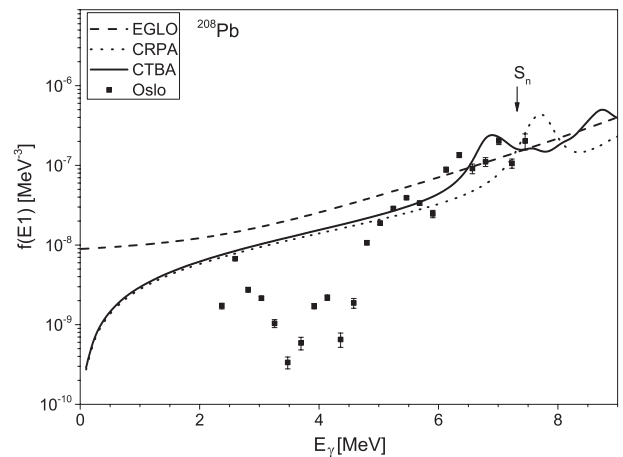


FIG. 5: E1 PSF for  $^{208}\text{Pb}$ . Dotted lines correspond to the self-consistent CRPA, solid lines to the CTBA (including PC), and dashed lines to the EGLO model [3]. Experimental data are taken from Ref. [29].

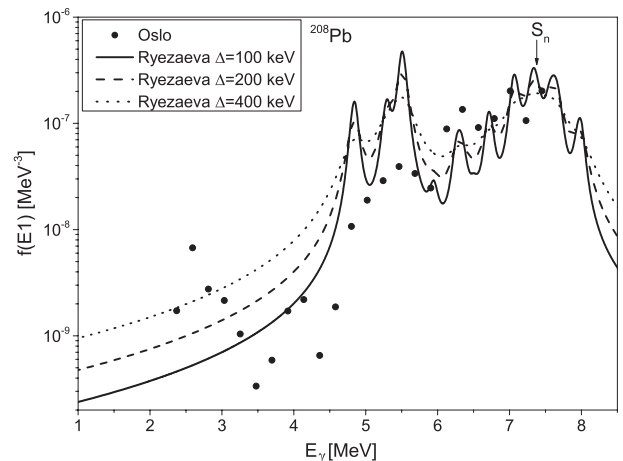


FIG. 6: Comparison of experimental strengths for  $^{208}\text{Pb}$ : the ( $^3\text{He}, ^3\text{He}'\gamma$ ) reactions method [29] and nuclear resonance fluorescence technique [30]. The lowest  $1^-$ -level of the data [30] is 4.84 MeV. It was smoothed by us with three different values of the smoothing parameter  $\Delta$ . See text for details.

200 keV has been used in the calculations). However, a large disagreement with experimental data is found at  $E < 5$  MeV. As one can see from Ref. [30], where the transitions between ground and excited states have been measured, the beginning of the  $1^-$  excitation spectrum is 4.84 MeV, i.e. there is no  $1^-$  transitions between ground and excited states below 4.84 MeV. This result is understandable since in the doubly-magic  $^{208}\text{Pb}$  there is no single-particle or two-phonon E1 transitions for  $E < 5$  MeV.

In order to obtain some additional information we have compared two sets of experimental data for  $^{208}\text{Pb}$  (see Fig. 6): 1) the PSF data from Ref. [29] where the transitions between ground and excited states as well as between excited states contribute and 2) the data [30] for

the  $B(E1)$  values for the transitions between ground and excited states only. It is necessary to compare both sets of data with approximately the same smoothing. So, taking into account the 200 keV resolution in the experimental data [29], we smoothed the data [30] with three smoothing parameters 100, 200 and 400 keV according to the following equation

$$f(E1, \omega) = \frac{8}{27(\hbar c)^3} \sum_s B(E1)_s \frac{\Delta}{(\omega - E_s)^2 + \Delta^2/4}. \quad (1)$$

As expected, we obtained a rough agreement between both sets of experimental data at  $E > 4.84$  MeV. Thus, one can think that the excitations observed in Ref. [29] at  $E < 4.84$  MeV are caused mainly by transitions between excited states. However, it is necessary to underline that the mechanisms of the reactions used in Refs. [29] and [30] are very different and, what is important here, the data from the Oslo  $^{208}\text{Pb}$  experiment [29] may suffer from a factor of 2 uncertainties due to low level density below the particle separation threshold<sup>1</sup>.

#### IV. NEUTRON RADIATIVE CAPTURE

##### A. Semi-magic compound $^{116}\text{Sn}$ and $^{120}\text{Sn}$

In Figs. 7 and 8, we present the radiative neutron capture cross sections estimated with the Hauser-Feshbach reaction code TALYS [15] on the basis of the newly determined gamma-strength function. Similar results are obtained if use is made of the EMPIRE reaction code [14]. The calculations were performed with different NLD models, including the back-shifted Fermi gas model [31], the Generalized Superfluid model (GSM) [3] and the HFB plus Combinatorial model [32, 33] (see Sect. VII). The NLD is constrained by experimental neutron spacings and low-lying states, whenever available [4]. As seen in Figs. 7-8, the agreement with experiment is only possible when the PC is taken into account [38]. QRPA approach clearly underestimates the strength at low energies. This deficiency is often cured by empirically shifting the QRPA strength to lower energies and broadening the distribution [1, 39].

##### B. Double-magic $^{132}\text{Sn}$ and $^{208}\text{Pb}$

In Figs. 9 and 10 the neutron radiative capture cross sections are shown for the compound  $^{132}\text{Sn}$  and  $^{208}\text{Pb}$ . Note that in Fig.10, we do not compare our results with the available  $^{207}\text{Pb}(n,\gamma)^{208}\text{Pb}$  cross section [40, 41] because these low-energy data (two points) are in the discrete resonance energy region. We see a large difference

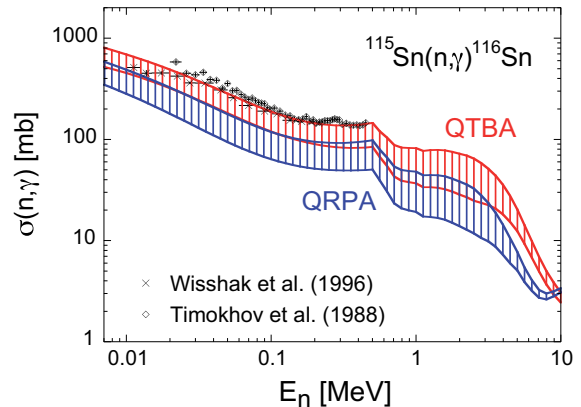


FIG. 7:  $^{115}\text{Sn}(n,\gamma)^{116}\text{Sn}$  cross section calculated with the QRPA (blue) and QTBA (red) PSF. The uncertainty bands depict the uncertainties affecting the NLD predictions [3, 31–33].  $E_n$  is the neutron energy. Experimental cross sections are taken from Refs. [34, 35].

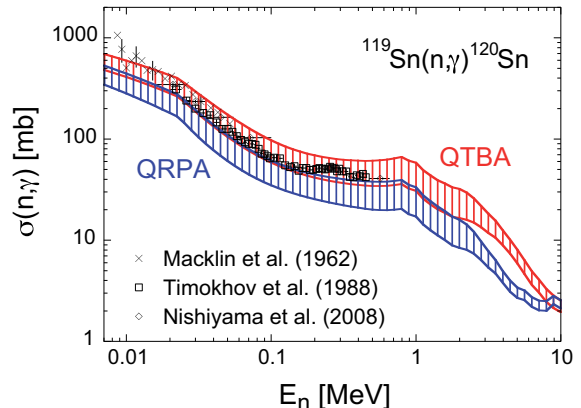


FIG. 8: Same as Fig. 7 for  $^{119}\text{Sn}(n,\gamma)^{120}\text{Sn}$ . Experimental cross section are taken from Refs. [34, 36, 37]

between the results obtained with the GSM and other NLD models (EMPIRE-specific and HFB plus combinatorial), namely, the GSM  $(n,\gamma)$  cross section is about one order of magnitude larger for neutrons up to energies of 2 MeV and 10 MeV for the compound  $^{132}\text{Sn}$  and  $^{208}\text{Pb}$ , respectively. There is no noticeable difference between the results obtained with phenomenological EMPIRE-specific and microscopic HFB plus combinatorial NLD models. A detailed discussion about these results will be presented somewhere else.

#### V. CAPTURE GAMMA-RAY SPECTRA

In Ref. [37], neutron capture gamma-ray spectra of  $^{117}\text{Sn}$  and  $^{119}\text{Sn}$  have been measured. With the use of EMPIRE and in order to compare them with theoretical predictions, we divide our results for gamma-ray spectra

<sup>1</sup> Private communications with the Oslo group

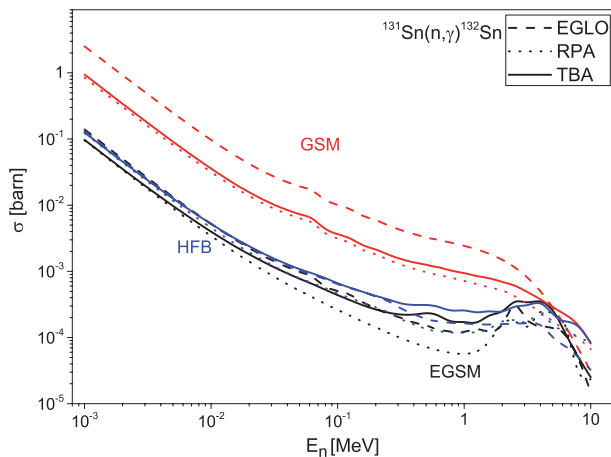


FIG. 9:  $^{131}\text{Sn}(n,\gamma)^{132}\text{Sn}$  cross section calculated with the EGLO (dashed), RPA (dotted) and TBA (solid) PSFs. The red, black and blue curves are obtained with the GSM, EMPIRE-specific and HFB plus combinatorial NLD models, respectively

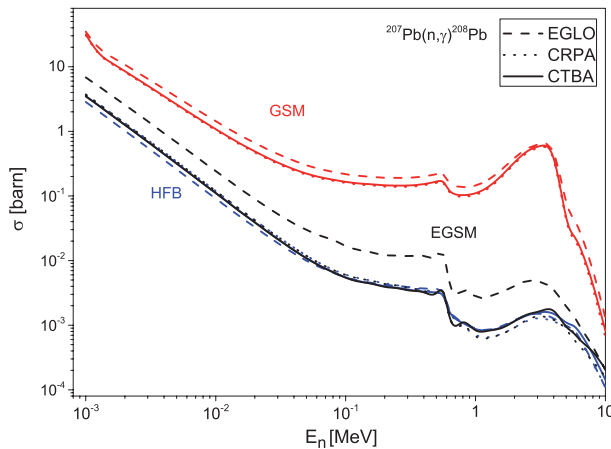


FIG. 10: The same as for Fig.9, but for the  $^{207}\text{Pb}(n,\gamma)^{208}\text{Pb}$  cross section calculated with the EGLO (dashed), CRPA (dotted) and CTBA (solid) PSFs.

in mb/MeV units by the capture cross sections at  $\langle E_n \rangle = 52$  keV and  $\langle E_n \rangle = 570$  keV for  $^{119}\text{Sn}$  (Fig. 11) (The case of  $\langle E_n \rangle = 46$  keV and  $\langle E_n \rangle = 550$  keV for  $^{117}\text{Sn}$  has been considered in Ref. [42]). In other words, we did not consider here the incident neutron energy spectra and took the neutron average energy of 52 keV given by the authors of Ref. [37]. The neutron cross sections are calculated with EMPIRE for three theoretical PSF models, EGLO, QRPA and QTBA. The comparison with experiment [37] is presented for two NLD models, namely the GSM (Fig. 11) and the microscopic HFB plus combinatorial model [32] (Fig. 12). One can see from Figs. 11 and 12 that the EGLO and QTBA predictions reproduce experimental data better than QRPA and that the detailed structures are also better described by QTBA than by EGLO.

As compared with the phenomenological GSM NLD model, the agreement with experiment is a little better for the microscopic HFB+combinatorial NLD model. Our results also show that the PC contribution is noticeable. For all three PSF variants some structures have been found but the QTBA approach describes them a little better.

TABLE II: Multiplicities of capture  $\gamma$ -rays ( $\gamma$ -rays/capture) of  $^{117,119}\text{Sn}$  calculated at  $E_\gamma > 0.6$  MeV. For each approach (EGLO, QRPA and QTBA) two NLD models are considered: the phenomenological GSM [3] (first line) and the microscopic HFB plus combinatorial model [32] (second line).

Nuclei	$E_n$	EGLO	QRPA	QTBA	Exp.
$^{117}\text{Sn}$	46 keV	3.64	3.32	2.99	3.45 (9)
		3.86	3.40	3.12	
$^{117}\text{Sn}$	550 keV	4.03	3.66	3.39	3.80 (20)
		3.48	4.24	3.73	
$^{119}\text{Sn}$	52 keV	3.57	3.23	2.96	3.31 (16)
		3.74	3.28	3.03	
$^{119}\text{Sn}$	570 keV	3.96	3.55	3.26	3.66 (19)
		4.11	3.59	3.33	

For completeness and to compare with the available experimental data [37], the calculation of multiplicity of observed capture gamma-rays at  $E > 0.6$  MeV has been performed for two target nuclei  $^{117}\text{Sn}$  and  $^{119}\text{Sn}$  by integrating the gamma-ray spectra with respect to the gamma-ray energy (see Table II). Two NLD models have been considered, namely the GSM (first line) and HFB plus combinatorial model (second line). One can see that for the QTBA case the use of HFB+combinatorial model increases the multiplicity values in the right direction but not significantly. As compared with the QRPA case, the inclusion of the PC decreases the multiplicities. Probably, the account for the energy spectra of the incident neutrons can improve the agreement with experiment.

We have also performed the capture gamma-ray spectrum calculations for the unstable  $^{68}\text{Ni}$  at the neutron energy of 100 keV (see Fig. 13). Here one can see a large difference between results with our two microscopic and the phenomenological EGLO PSF models; this confirms the necessity of using the microscopic approach for unstable nuclei. A similar situation is found if use is made of the GSM NLD model in Ref. [42].

## VI. AVERAGE RADIATIVE WIDTHS

To test the low-lying strength predicted within the various existing models, we also consider the average radiative widths of neutron resonances  $\Gamma_\gamma$ , known to be a property of importance in the description of the  $\gamma$ -decay from high-energy nuclear states. This quantity is used in nuclear reaction calculations, in particular, to normalize the PSF around the neutron threshold and is defined by

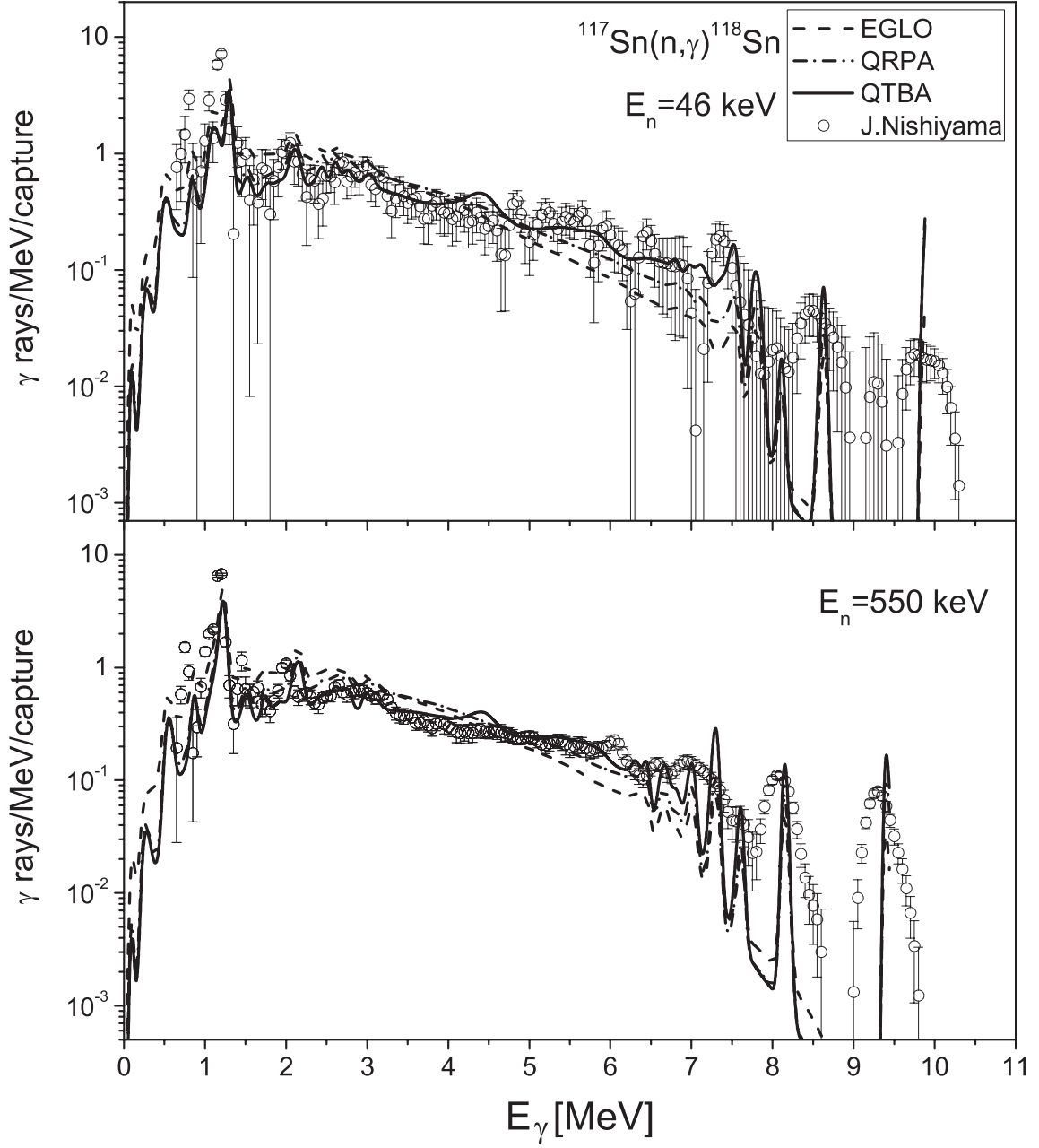


FIG. 11: Gamma-ray spectra from  $^{117}\text{Sn}(n,\gamma)^{118}\text{Sn}$  for the neutron energies of 52 keV (upper panel) and 570 keV (lower panel) calculated with EMPIRE and the phenomenological GSM NLD model [3]. Experimental data was taken from [37]. See text for details

[19]:

$$\Gamma_\gamma = \sum_{I=|J-1|}^{J+1} \int_0^{S_n} \epsilon_\gamma^3 f_{E1}(\epsilon_\gamma) \frac{\rho(S_n - \epsilon_\gamma, I)}{\rho(S_n, J)} d\epsilon_\gamma, \quad (2)$$

where  $\rho$  is the NLD and  $J$  the spin of the initial state in the compound nucleus. Extended compilation of experimental data for  $\Gamma_\gamma$  can be found in Refs. [2–4].

### A. Sn and Ni semi-magic isotopes

We have calculated the  $\Gamma_\gamma$  values for 13 Sn and Ni isotopes on the basis of the EMPIRE code [14] for the 3 different PSF models, namely EGLO, our SLy4+QRPA and the present QTBA, together with different NLD prescriptions, namely the GSM [3] and the microscopic HFB plus combinatorial model [32], see Table III. The predictions are compared with experimental data [2], whenever available, and with existing systematics [3, 4]. As seen in Table III, the PC effect in stable nuclei significantly

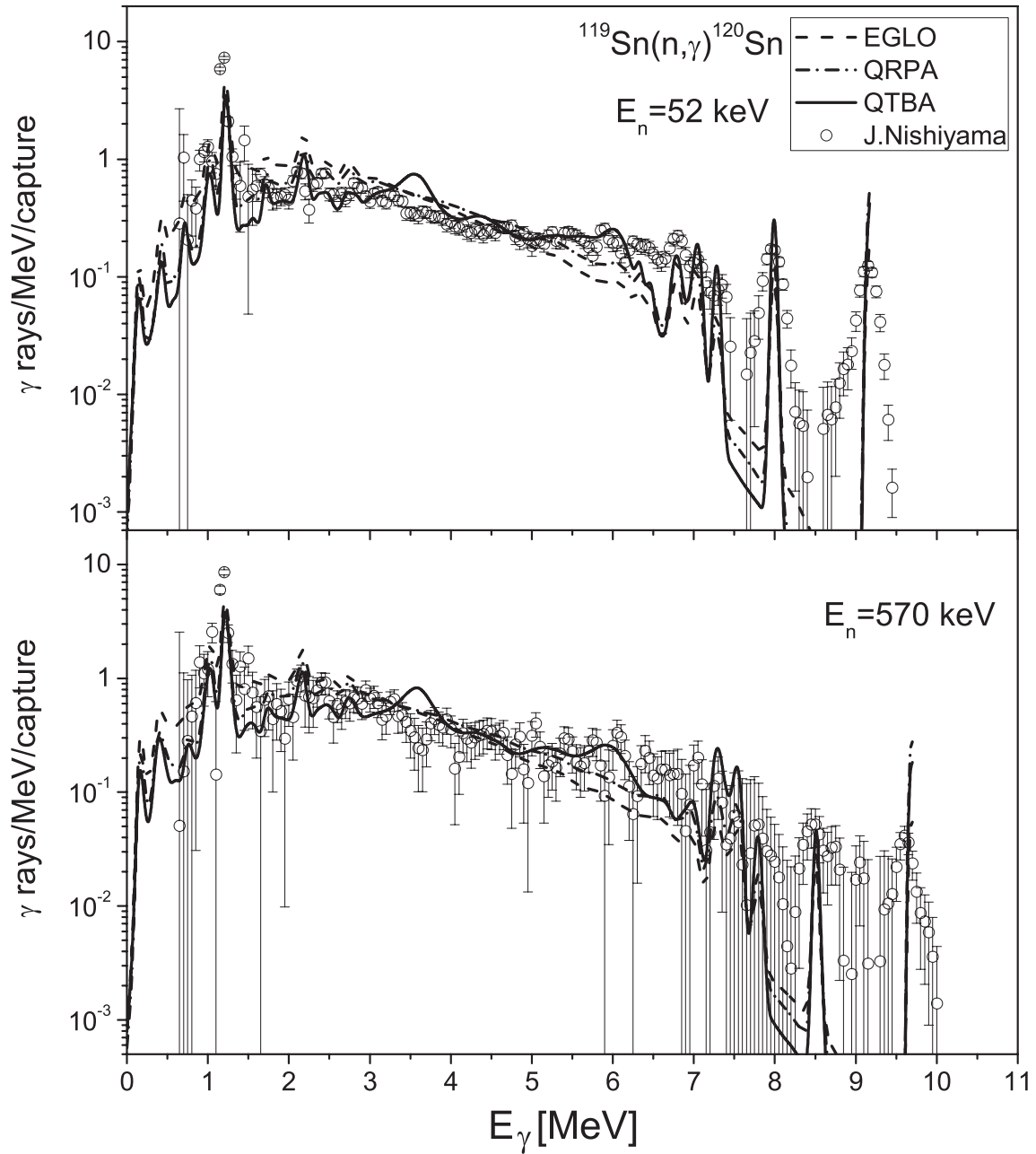


FIG. 12: Gamma-ray spectra from  $^{119}\text{Sn}(n,\gamma)^{120}\text{Sn}$  for the neutron energy of 52 keV and 570 keV. The microscopic HFB+combinatorial NLD model [32] has been used. Experimental data was taken from [37].

increases the QRPA contribution and improves the agreement with the systematics. Except for  $^{122}\text{Sn}$  and  $^{124}\text{Sn}$ , where the increase is limited, the PC leads to an enhancement of about 50 to 200%.

Our  $\Gamma_\gamma$  results for  $^{118}\text{Sn}$ ,  $^{120}\text{Sn}$ ,  $^{60}\text{Ni}$  and  $^{62}\text{Ni}$ , for which experimental data (not systematics) exists, are of special interest. On the basis of the QTBA strength and the microscopic HFB plus combinatorial NLD [32], we obtain a good agreement with experiment for  $^{60}\text{Ni}$ ,  $^{62}\text{Ni}$ , and reasonable for  $^{118}\text{Sn}$  and  $^{120}\text{Sn}$ .

Note that on top of the E1 strength, an M1 contribu-

tion following the recommendation of Ref. [4] is included in the calculation of  $\Gamma_\gamma$ . The M1 resonance contribution to  $\Gamma_\gamma$  has been estimated in Table III using the GSM and HFB plus combinatorial NLD models and the standard Lorentzian parametrization [4] with a width  $\Gamma = 4$  MeV (note that such a large  $\Gamma$  value is open to question, as discussed in Ref. [43]). Such a contribution is found to be of the order of (10-12)% of the values in the first line of Table. III for Sn isotopes and 4, 3, 22 and 16% for  $^{58}\text{Ni}$ ,  $^{62}\text{Ni}$ ,  $^{68}\text{Ni}$  and  $^{72}\text{Ni}$ , respectively. In our opinion, the question of the M1 contribution to  $\Gamma_\gamma$  requires some



TABLE III: Average radiative widths  $\Gamma_\gamma$  (meV) for s-wave neutrons. For each approach (EGLO, QRPA and QTBA) two NLD models are considered: the phenomenological GSM [3] (first line) and the microscopic HFB plus combinatorial model [32] (second line). See text for details.

	$^{110}\text{Sn}$	$^{112}\text{Sn}$	$^{116}\text{Sn}$	$^{118}\text{Sn}$	$^{120}\text{Sn}$	$^{122}\text{Sn}$	$^{124}\text{Sn}$	$^{132}\text{Sn}$	$^{136}\text{Sn}$	$^{58}\text{Ni}$	$^{60}\text{Ni}$	$^{62}\text{Ni}$	$^{68}\text{Ni}$	$^{72}\text{Ni}$	$^{208}\text{Pb}$
EGLO	147.4	105.5	72.9	46.6	55.0	56.6	49.9	398	11.1	1096	474	794	166	134	10.6
	207.9	160.3	108.9	106.7	124.3	110.2	128.7	4444	295.0	2017	1882	1841	982.2	86.4	2734
QRPA	45.6	34.4	30.4	22.1	23.8	27.9	22.3	133	11.2	358	594	623	75.4	83.8	4.4
	71.0	49.7	44.3	40.3	43.0	50.1	68.9	4279	447.8	450.8	1646	490.9	406.4	46.7	2973
QTBA	93.5	65.7	46.8	33.1	34.1	35.8	27.9	148	12.3	1141	971	1370	392	154	4.6
	119.9	87.0	58.4	58.1	61.5	64.0	84.8	4259	509.2	1264	2800	2117	2330	53.8	2448
Exp. [2]				117 (20)	100 (16)						2200 (700)	2000 (300)			
[3]				80 (20)							2200 (700)	2200 (700)			
M1	13.0	9.6	8.9	6.1	6.6	7.3	4.9	40.9	1.3	46.1	32	23.2	36.0	49.6	0.79
	29.1	18.1	18.5	13.2	13.4	13.1	15.5	341	87.2	17.0	52	31.8	81.6	27.5	5.25
System.	112	109	107	106	105	104	103	85	73	2650	1900	1300	420	320	3770

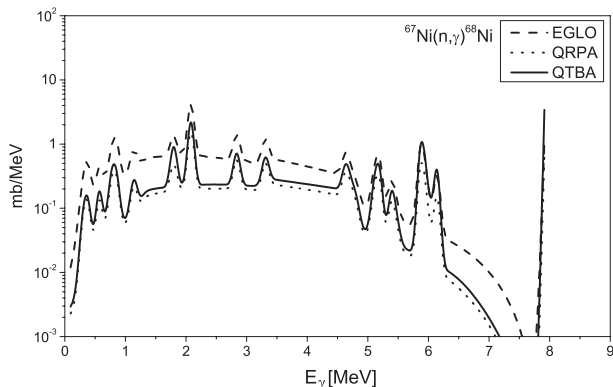


FIG. 13: Gamma-ray spectra from  $^{68}\text{Ni}(n,\gamma)$  at the neutron energy of 100 keV. The microscopic HFB+combinatorial NLD model [32] has been used.

additional consideration.

The agreement of the  $\Gamma_\gamma$  values with experiment is found to deteriorate if use is made of the EGLO or QRPA strengths, but also of the GSM NLD. One can also see that for stable nuclei, the combinatorial NLD model results are in a better agreement with the systematics [3] than those obtained with the GSM model. As far as the EGLO model is concerned, we see that similar conclusions can be drawn.

### B. Doubly-magic $^{132}\text{Sn}$ and $^{208}\text{Pb}$

Unfortunately, the experimental data are very scarce for the doubly-magic nuclei  $^{132}\text{Sn}$  and  $^{208}\text{Pb}$ . However, as shown in Table III, we find, for  $^{208}\text{Pb}$ , a reasonable agreement between EMPIRE predictions and the  $\Gamma_\gamma$  systematics [2], at least with the HFB + combinatorial NLD model, not with GSM one (nor with the EMPIRE-specific NLD). For the average resonance s-wave level spacings  $D_0$ , GSM gives 0.0044 keV, EMPIRE-specific model 32 keV and HFB+Combinatorial model 37.6, the two last to being in agreement with the ex-

perimental value of  $30 \pm 8$  keV. The GSM in EMPIRE clearly produces unreasonably small value for  $D_0$ . EMPIRE also gives a very small contribution of the M1 resonance to the  $\Gamma_\gamma$  values for  $^{208}\text{Pb}$  both with the GSM and HFB+combinatorial NLD models, namely 0.02% and 0.1% of the systematics value of  $\Gamma_\gamma = 3770$  meV [2], respectively (Table III).

## VII. NLD MODELS

Since Bethe's pioneering work [44], many studies have been devoted to the evaluation of the NLD. The so-called partition function method is by far the most widely used technique for calculating level densities, particularly in view of its ability to provide simple analytical formulae. In its simplest form, the NLD is evaluated for a gas of non-interacting fermions confined to the nuclear volume and having equally spaced energy levels. Such a model corresponds to the zeroth order approximation of a Fermi gas model and leads to very simple analytical, though unreliable, expressions for the NLD.

In an attempt to reproduce the experimental data, various phenomenological modifications to the original analytical formulation of Bethe have been suggested, in particular to allow for shell, pairing and collective effects. This led first to the constant temperature formula, then to the shifted Fermi gas model, and later to the popular back-shifted Fermi gas (BSFG) model [45, 46]. To describe the shell effect, other empirical or phenomenological improvements to the Fermi formula have been attempted by introducing an energy dependence to the shell energy shift [47, 48]. To account for a more realistic pairing correction, analytical expressions have been derived from the BCS formulation, but at the expense of numerous approximations [49]. This includes the GSM approach [50] or the semi-classical approximation [49]. In such an analytical approach, collective rotational and/or vibrational effects are often not treated explicitly.

Some attempts to include all the shell, pairing and deformation effects analytically in the NLD formula are

found in Refs. [49–51]. However, drastic approximations are usually made in deriving such analytical NLD formulae and their shortcomings in matching experimental data are overcome by empirical parameter adjustments. For practical applications, the available experimental information can not be omitted and global formulae are tuned by a local determination of the free parameters for each nucleus. To do so, the NLD formula is renormalized on existing experimental data (mainly low-lying levels and s-wave neutron resonance spacings). So far, only simple analytical formulae of the BSFG type have been renormalized and used in practical applications [50–52].

Several of the approximations used to obtain the NLD expressions in an analytical form can be avoided by quantitatively taking into account the discrete structure of the single-particle spectra associated with realistic effective potentials. This approach leads to the so-called microscopic statistical model (e.g.[53–56]). The NLD computed with this technique is the exact result that the analytical approximation tries to reproduce. This approach has the advantage of treating in a natural way shell, pairing and deformation effects on all the thermodynamic quantities. However, the statistical model is not free from uncertainties. In particular some inherent problems related to the choice of the single-particle configuration and pairing force remain. The treatment of the collective enhancement factor as well as the deformation effects at increasing energies and for transient nuclei are usually treated in a phenomenological way. The global microscopic NLD prescription within the statistical approach based on the Hartree-Fock-BCS (HFBCS) ground state properties [56] has proven the capacity of microscopic models to compete with phenomenological models in the reproduction of experimental data and consequently to be adopted for practical applications. However, this statistical approach still presents the drawback of not describing the parity dependence of the NLD, nor the discrete (i.e non-statistical) nature of the excited spectrum at low energies.

Other various microscopic models have been proposed, including, for example, the combinatorial model [57, 58], the spectral distribution approach [59], Monte-Carlo [60] and quantum Monte-Carlo models, including correlations beyond the mean-field approximation [61–63]. Among those, the combinatorial approach has been the most developed so far and it was demonstrated that such an approach can clearly compete with the statistical approach in the global reproduction of experimental data [32, 64–66]. One of the advantages of this approach is to provide not only the energy, spin and parity dependence of the NLD, but also the partial particle-hole level density that cannot be extracted in any satisfactory way from the statistical approaches. At low energies, the combinatorial predictions also provide the non-statistical limit where by definition the statistical approach cannot be applied.

The combinatorial method consists in using the single-particle level schemes obtained from constrained axially symmetric HFB method to construct incoherent particle-

hole (ph) state densities as functions of the excitation energy, the spin projection (on the intrinsic symmetry axis of the nucleus) and the parity. Once these incoherent ph state densities are determined, collective effects have to be included. In Ref. [65], the choice was made to describe the vibrational effects by multiplying the total level densities by a phenomenological enhancement factor [50, 67] once rotational bands had been constructed. The resulting NLD were found to reproduce very well the available experimental data (i.e. both the cumulated low energy discrete level histograms and the s- and p-wave resonances mean spacings at the neutron binding energy). However, it was clear that the phenomenological treatment of vibrational effects needs to be replaced by a sounder treatment. Indeed, rotational bands built on purely vibrational band-heads are well established and can clearly not be described if the vibrational enhancement occur once the rotational bands are constructed as done in Ref. [65]. Feedback from fission cross section calculations also suggested this lack of vibrational states at low energies [68].

To improve the reliability of the microscopic prediction of NLD, the vibrational enhancement factor was later included in the combinatorial approach explicitly by allowing for phonon excitations using the boson partition function of Ref. [64] which includes quadrupole, octupole as well as hexadecapole vibrational modes. Whereas single-particle levels are theoretically obtained for any nucleus, phonon's energies are taken from experimental information when available or from analytical expressions [32]. Once the vibrational and incoherent ph state densities are computed, they are folded to deduce the total state and the level densities are then deduced exactly like in Ref. [65]. To account for the damping of vibrational effects at increasing energies, the folding was restricted to the ph configurations having a total exciton number (i.e. the sum of the number of proton and neutron particles and proton and neutron holes)  $N_{ph} \leq 4$ . This restriction stems from the fact that a vibrational state results from a coherent excitation of particles and holes, and that this coherence vanishes with increasing number of ph involved in the description. Therefore, if one deals with a ph configuration having a large exciton number, one should not simultaneously account for vibrational states which are clearly already included as incoherent excitations.

The combinatorial model was further improved [66] for deformed nuclei by taking into account the transition to sphericity coherently on the basis of a temperature-dependent Hartree-Fock calculation. This approach provides at each temperature the structure properties needed to build the level densities. The derived NLDs were shown to provide fairly good results when compared with experimental data [66].

As an illustration of the different predictions, we compare in Fig. 14 the experimental s-wave spacings [3, 4] with those obtained with the BSFG NLD [69], the microscopic statistical HFBCS model [56] and the HFB plus combinatorial model [32]. Rather similar accura-

cies (with an average deviation corresponding to a factor of 2) are obtained over the whole nuclear chart where data is available. As shown in Refs. [65, 66], the HFB plus combinatorial model also gives satisfactory extrapolations to low energies, in particular with respect to the measured cumulative number of levels and the total level density extracted by the Oslo group from the analysis of particle- $\gamma$  coincidence in the ( $^3\text{He}, \alpha\gamma$ ) and ( $^3\text{He}, ^3\text{He}'\gamma$ ) reactions [29].

The corresponding NLD tables [32] are available to the scientific community at the website <http://www-astro.ulb.ac.be>. The tables include the spin- and parity-dependent NLD for more than 8500 nuclei ranging from  $Z = 8$  to  $Z = 110$  for a large energy and spin grid ( $U = 0$  to 200 MeV and the lowest 30 spins). No simple analytical fit to the tabulated NLD is given to avoid losing the specific microscopic characteristics of the model. It should be stressed that the combinatorial NLD cannot be approximated by a simple BSFG-type formula, except at very-high energies (above roughly 100 MeV), where the shell, pairing and deformation effects disappear.

One major advantage of the combinatorial method is its non-statistical feature which enables to obtain realistic parity and spin distributions, especially at low energies where the statistical limit fails. Another advantage lies in the parity dependence which can hardly be estimated within the statistical approach. It should be noted that the non-equipartition of parities can have a non-negligible impact, in particular on radiative capture cross sections [65]. Concerning the spin distribution, the combinatorial approach provides with NLD that may significantly deviate from the usually adopted Wigner law, in particular at low energy since the number of levels is not high enough to reach a Gaussian distribution. Such deviations can play a key role when considering the decay to spin isomers at low energies [70], since high-spin populations are usually underestimated within the statistical approach, leading to an underestimate of the decaying probability to high spin levels. Yet, the combinatorial method can still be improved to better account for collective effects, especially at increasing excitation energies. A first attempt has been made to account for the variations of nuclear structure properties with increasing excitation energy thanks to a temperature-dependent HFB calculation [66]. The damping of the vibrational enhancement can also be inspired from the results obtained from more microscopic approaches, such as the shell-model Monte Carlo method [63].

### VIII. CONCLUSION

The PSFs and PDR in stable and unstable Ni and Sn isotopes as well as in doubly-magic  $^{132}\text{Sn}$  and  $^{208}\text{Pb}$  have been calculated within the microscopic self-consistent version of the extended theory of finite fermi systems which, in addition to the standard QRPA approach, in-

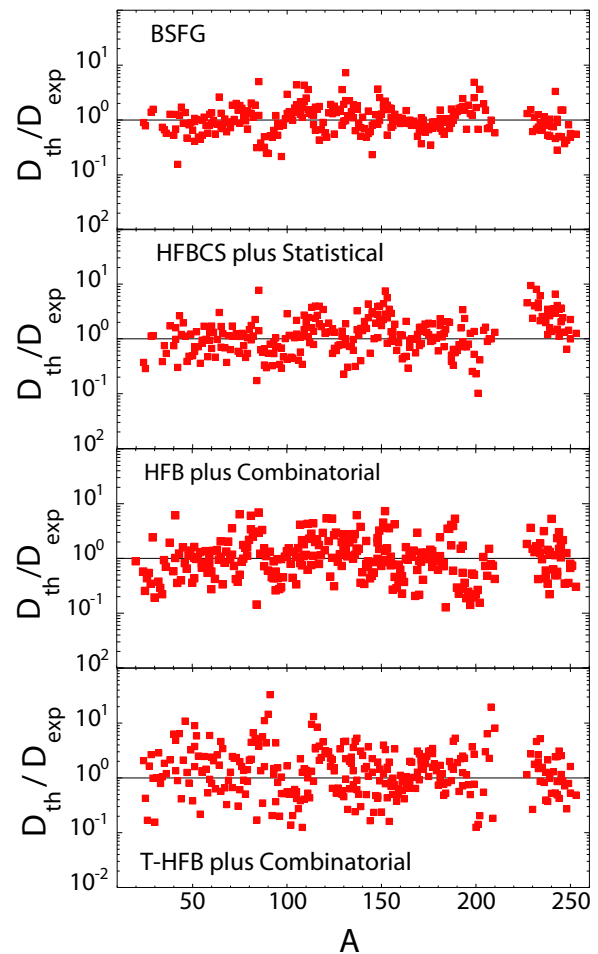


FIG. 14: Upper panel: Ratio of BSFG [69] ( $D_{th}$ ) to the experimental ( $D_{exp}$ )  $s$ -wave neutron resonance spacings compiled in Refs. [3, 4]. Middle upper panel: Same with the HFBCS plus Statistical approach of Ref. [56]. Middle lower panel: same with the HFB plus combinatorial model of Ref. [32]. Lower panel: same with the T-dependent HFB plus combinatorial model of Ref. [66].

cludes the PC effects. The Skyrme force SLy4 was used. An update on modern microscopic models of NLD based on the self-consistent HFB plus combinatorial method was also given.

The microscopically obtained PSFs were compared with the available experimental data on E1 strength as well as on nuclear reaction properties using the reaction codes EMPIRE and TALYS. Average radiative widths, radiative neutron capture cross sections and capture gamma-ray spectra have been calculated taking the PC into account and using various NLD models to assess the related uncertainties.

The essential and new ingredient of our microscopic QTBA approach is the inclusion of the PC effect. First, in contrast with phenomenological PSFs, which have no structures, it is required for the explanation of detailed and observed structures in the PSFs in the energy re-

gion below the nucleon separation energy. Second, the quantitative PC contribution significantly improves the agreement with existing experimental data, both for the PSFs, as shown for some Sn isotopes (Figs.1 and 2), and for average radiative widths  $\Gamma_\gamma$  (Table III), which are increased by about 50-200% by the PC. Here, the  $\Gamma_\gamma$  values are increased always toward better agreement with experiment or systematics, and the PC inclusion results in a reasonable description of the available experiment. We have also shown that the agreement with experimental  $^{115}\text{Sn}(n,\gamma)^{116}\text{Sn}$  and  $^{119}\text{Sn}(n,\gamma)^{120}\text{Sn}$  cross sections is only possible when the PC is taken into account (Figs. 7 and 8).

Many observables related to the PSF remain however also sensitive to the adopted NLD model. The HFB plus combinatorial NLD model can clearly compete with the statistical approach in the global reproduction of experimental data, not to mention its higher predictive power. It provides energy, spin and parity dependence of the NLD and at low energies describes the non-statistical limit. We have shown that predictions can be improved

with such a microscopic approach, in particular with respect to the phenomenological GSM.

The main conclusion of the work is that microscopic approaches are necessary to calculate NLD as well as radiative nuclear reaction characteristics and can now replace more phenomenological models, not only for the description and interpretation of experimental data, but also for applications, such as nuclear astrophysics or nuclear engineering.

## ACKNOWLEDGEMENTS

The work has been partly supported within the cooperation between INPE NRNU MIPHI and Institute für Kernphysik FZ Jülich. S.K. acknowledges useful discussions with Drs. V. Furman, T.Katabuchi, V.Pronyaev, A.Voinov. The authors acknowledge discussions of the  $^{208}\text{Pb}$  results with Therese Renstrom and Profs. S. Siem, M. Guttormsen and A.C. Larsen from the Oslo group. SG is FNRS Research Associate.

- 
- [1] S. Goriely, E. Khan, V. Samyn, Nucl. Phys. A **739**, 331 (2004).
- [2] S.F. Mughabghab, *Atlas of neutron Resonances, Resonance Parameters and Thermal Cross Sections Z=1-100* (Elsevier, Amsterdam, 2006).
- [3] T. Belgia, O. Bersillon, R. Capote *et al.*, *Handbook for Calculations of Nuclear Reaction Data, RIPL-2*, IAEA-TECDOC-1506 (IAEA, Vienna, 2006) [<http://www-nds.iaea.org/RIPL-2/>].
- [4] R. Capote, M. Herman, P. Obložinsky *et al.*, Nuclear Data Sheets **110**, 3107 (2009). See also <https://www-nds.iaea.org/RIPL-3>.
- [5] D.M. Brink, Ph.D Thesis, Oxford University (1955).
- [6] O. Wieland, A. Bracco, F. Camera *et al.*, Phys. Rev. Lett. **102**, 092502 (2009).
- [7] D. Savran, T. Aumann, A. Zilges, Prog. Part. and Nucl. Phys. **70**, 210 (2013).
- [8] S.P. Kamedzhiev, A.V. Avdeenkov, O.I. Achakovskiy, Phys. Atom. Nucl. **77**, 1303 (2014).
- [9] N. Paar, D. Vretenar, E. Khan, G. Colo, Rep. Prog. Phys. **70**, 691 (2007).
- [10] H.K. Toft, A. C. Larsen, U. Agvaanluvsan *et al.*, Phys. Rev. C **81**, 064311 (2010).
- [11] H.K. Toft, A. C. Larsen, A. Bürger *et al.*, Phys. Rev. C **83**, 044320 (2011).
- [12] R. Schwengner, R. Massarczyk, G. Rusev *et al.*, Phys. Rev. C **87**, 024306 (2013).
- [13] H. Utsunomiya, S. Goriely, M. Kamata *et al.*, Phys. Rev. C **84**, 055805 (2011).
- [14] M. Herman, R. Capote, B.V. Carlson *et al.*, Nucl. Data Sheets, **108** (2007) 2655-2715. See also <http://www.nndc.bnl.gov/empire/index.html>.
- [15] A.J. Koning and D. Rochman, Nuclear Data Sheets **113**, 2841 (2012).
- [16] S.Kamedzhiev, J. Speth, G. Tertychny, Phys. Rep. **393**, 1 (2004).
- [17] A. Avdeenkov, S. Goriely, S. Kamedzhiev, S. Krewald, Phys. Rev. C **83**, 064316 (2011).
- [18] V.G. Soloviev, Ch. Stoyanov and V.V. Voronov, Nucl. Phys. **A304**, 503 (1978).
- [19] T.S. Belanova, A.V. Ignatyuk, A.B. Pashchenko, V.I. Plyaskin, Handbook *Radiative neutron capture*, 1986.
- [20] V. Tselyaev, Phys. Rev. C **75**, 024306 (2007).
- [21] E. Chabanat, P. Bonche, P. Haensel, Nucl. Phys. A **635**, 231 (1998).
- [22] K.Bennaceur and J. Dobaczewski, Comp. Phys. Comm, **168**, 96 (2005).
- [23] V. V. Varlamov, N. N. Peskov, D. S. Rudenko, and M. E. Stepanov, Vopr. At. Nauki Tekh., Ser. Yad. Konstany **1**, 2 (2003).
- [24] S. C. Fultz, B. L. Berman, J. T. Coldwell *et al.*, Phys. Rev. **186**, 1255 (1969).
- [25] A. Leprêtre, H. Beil, R. Bergere *et al.*, Nucl. Phys. A **219**, 39 (1974).
- [26] E. Litvinova, P. Ring, V. Tselyaev, Phys. Rev. Lett. **105**, 022502 (2010).
- [27] N. Lyutorovich, V. Tselyaev, J. Speth *et al.*, Phys. Lett. B **749**, 292 (2015).
- [28] P. Adrich, A. Klimkiewicz, M. Fallot *et al.*, Phys. Rev. Lett. **95**, 132501 (2005).
- [29] N.U.H. Syed, M. Guttormsen, F. Ingebretsen *et al.*, Phys. Rev. C **79**, 024316 (2009).
- [30] N. Ryezayeva, T. Hartmann, Y. Kalmykov *et al.*, Phys. Rev. Lett. **89**, 272502 (2002).
- [31] A.J. Koning, S. Hilaire, S. Goriely, Nucl. Phys. A **810**, 13 (2008).
- [32] S. Goriely, S. Hilaire, A.J. Koning, Phys. Rev. C **78**, 064307 (2008).
- [33] S. Hilaire, M. Girod, S. Goriely and A.J. Koning, Phys. Rev. C **86**, 064317 (2012).
- [34] V.M. Timokhov *et al.*, Fiz.-Energ Institut, Obninsk Reports No.1921 (1988).

- [35] K. Wisshak, *et al.*, Phys. Rev. C **54**, 1451 (1996).
- [36] R.L. Macklin, T. Inada, J.H. Gibbons, Washington AEC Office Reports, No.1041, p.30 (1962).
- [37] J. Nishiyama, M. Igashira, T. Ohsaki *et al.*, J. Nucl. Sci. Technol. (Tokyo) **45**, 352 (2008).
- [38] O. Achakovskiy, A. Avdeenkov, S. Goriely *et al.*, Phys. Rev. C **91**, 034620 (2015).
- [39] S. Goriely, E. Khan, Nucl. Phys. A **706**, 217 (2002).
- [40] R.C. Greenwood, C.W. Reich, Phys. Rev. C **4**, 2249 (1971).
- [41] O.A. Wasson, R.E. Chrien, R.C. Greenwood, Rept. USNDC-7 P36.
- [42] O.I. Achakovskiy, A.V. Avdeenkov, S.P. Kamerdzhev and D.A. Voitenkov, in Proceedings of the International Seminar on Interaction of Nuclei with Nucleons, ISINN22 (Dubna, May 2730, 2014), p. 207.
- [43] S.P. Kamerdzhev, S.F. Kovalev, Phys. At. Nucl. **69**, 418 (2006).
- [44] H.A. Bethe, Phys. Rev., **50**, 332 (1936).
- [45] A. Gilbert and A.G.W. Cameron, Can. J. Phys. **43** (1965) 1446.
- [46] J.R. Huizenga and L.G. Moretto, Ann. Rev. Nucl. Sci. **22** (1972) 427.
- [47] A.V. Ignatyuk, G.N. Smirenkin and A.S. Tishin, Sov. J. Nucl. Phys. **21** (1975) 255.
- [48] S.K. Kataria, V.S. Ramamurthy and S.S. Kappor, Phys. Rev. C **18** (1978) 549.
- [49] S. Goriely, 1996, Nuc. Phys. A **605** 28.
- [50] A.V. Ignatyuk, IAEA report, TEXDOC-1034, (1998).
- [51] A.J. Koning, S. Hilaire, S. Goriely, Nucl. Phys. A **810**, 13 (2008).
- [52] W. Dilg, W. Schantl, H. Vonach and M. Uhl, Nucl. Phys. A **217** (1973) 269.
- [53] P. Decowski *et al.*, Nuc. Phys. A **110** (1968) 129.
- [54] L.G. Moretto, Nuc. Phys. A **185**, (1972) 145.
- [55] M. Arnould, F. Tondeur, Proc. Conf. on nuclei far from stability, Helsingør, CERN 81-09, vol1, p.229 (1981).
- [56] P. Demetriou and S. Goriely, Nucl. Phys. A **695**, 95 (2001).
- [57] M. Hillman, J.R. Grover, Phys. Rev. **185** (1968) 1303.
- [58] S. Hilaire and J.P. Delaroche, *Nuclear Data for Science and Technology*, Italian Physical Society: Reffo *et al.* (eds), 1997, pp. 694.
- [59] J.B. French and K.F. Ratcliff, Phys. Rev. C **3** (1971) 94.
- [60] N. Cerf, Phys. Rev. C **49** (1994) 852; Phys. Rev. C **50** (1994) 836.
- [61] H. Nakada and Y. Alhassid, Phys. Rev. Lett. **79** (1997) 2939.
- [62] Y. Alhassid, S. Liu and H. Nakada, Phys. Rev. Lett. **83** (1999) 4265.
- [63] C. Özen, Y. Alhassid, H. Nakada, Phys. Rev. Lett. **110**, 042502 (2013).
- [64] S. Hilaire, J.P. Delaroche and M. Girod, Eur. Phys. J. A **12**, 169 (2001).
- [65] S. Hilaire and S. Goriely, Nucl. Phys. A, **779**, 63 (2006).
- [66] S. Hilaire, M. Girod, S. Goriely, A.J. Koning, Phys. Rev. C **86** 064317, (2012).
- [67] A.V. Ignatyuk, IAEA report, INDC(CCP)-233/L (1985).
- [68] M. Sin *et al.*, in *Nuclear Data for Science and Technology*, O. Bersillon *et al.* (eds); EDP Sciences, (2008) p. 313.
- [69] S. Goriely, J. Nucl. Sci. Technol. Suppl. **2**, 536 (2002).
- [70] S. Goko *et al.*, Phys. Rev. Lett. **96**, 192501 (2006).